ILASS 2008
Sep. 8-10, 2008, Como Lake, Italy

Paper ID ILASS08-11-4

COUNTERFLOW COMBUSTION MODELING OF CH_4/AIR AND CH_4/O_2 INCLUDING DETAILED CHEMISTRY

D. Urzica, E. Gutheil*

Interdisziplinäres Zentrum für Wissenschaftliches Rechnen, Universität Heidelberg
Im Neuenheimer Feld 368, 69120 Heidelberg, Germany

Email: urzica@iwr.uni-heidelberg.de, Phone: +49-6221-545729, Fax: +49-6221-546111
Email: gutheil@iwr.uni-heidelberg.de, Phone: +49-6221-546114, Fax: +49-6221-546111

ABSTRACT

The understanding of physical and chemical processes occurring in many applications in sciences and engineering is important to ensure stability and efficiency of their performance. Examples are the combustion process in direct-injection engines, gas turbine combustors, and liquid rocket propulsion systems. The objective of this paper is a numerical investigation of laminar CH_4/air as well as CH_4/O_2 flames in the counterflow configuration. These structures may be used in (spray) flamelet computations of turbulent combustion. The mathematical model is based on two-dimensional equations which are transformed into one-dimensional equations through use of a similarity transformation. The numerical simulation concerns the axi-symmetric configuration with an adaptive numerical grid for the gas phase. Detailed models of all relevant processes are employed; in particular, a detailed chemical reaction mechanism is used which comprises 35 species involving 294 elementary reactions. For the CH_4/air laminar flame, the obtained results are compared with results from literature to verify the model and the numerical scheme. The CH_4/O_2 laminar flame is studied for elevated pressures up to *2*MPa. Extinction strain rates are computed and the scalar dissipation rate is displayed. The library is ready for use in turbulent flamelet computations. Moreover, flames with different degrees of nitrogen dilution in the air stream are investigated. It appears that nitrogen dilution, pressure as well as strain rate have a pronounced effect on flame structures.

INTRODUCTION

In the last years, methane (CH_4) is considered an alternative fuel to hydrogen in liquid rocket propulsion systems. The so called 'green propellant' has become attractive because of its limited effect on environment compared to other hydrocarbons, and it has several advantages compared to hydrogen because of safety in transport and storage as well as high energy content.

There are two major research groups in Europe which experimentally investigate the CH_4/O_2 flames: ONERA in France and DLR Lampoldshausen in Germany.

Both ONERA's Mascotte test facility[2] and the DLR's M3 combustion chamber [7], which initially were developed for experimental investigations of liquid oxygen/gaseous hydrogen combustion (LOx/H_2) have been modified to allow for the study of LOx/CH_4. In their studies, pressure ranges from 0.1 to 5.5MPa, the injection temperature for LOx is 85K, and for liquid CH_4 it is 125K, hence both temperatures are cryogenic. A later study [3] concerns fuel rich conditions. Candel et al. [4] studied the flame structure of both LOx/CH_4 and LOx/H_2 in the transcritical range for a pressure range between 0.1 to 7MPa and a subcritical injection temperature of liquid oxygen. Combustion of cryogenic oxygen and methane injected at pressures between 4.5 and 6MPa were investigated experimentally in [5]. The coaxial injector delivers oxygen at a temperature of 85K and methane at a temperature of 120K or 288K. Stabilization of flames formed by cryogenic liquid oxygen/gaseous hydrogen or methane has been investigated through planar laser induced fluorescence (PLIF) of OH [6]. In the LOx/GH_2 experiments, injection conditions are transcritical, since the chamber pressure (6.3MPa) is above the critical value but the temperature (80K) is below the critical value. In the LOx/GCH_4 experiments, the chamber pressure (2MPa) and LOx injection temperature (80K) are below critical values.

In the DLR experiments [7], a comparison between spray combustion for coaxially injected CH_4/LOx and H_2/LOx, at similar injection conditions was performed where the Weber number and the momentum flux ratio were varied. In [8], experimental investigations on the development of LOx/CH_4 flames, especially ignition and flame stabilization - strongly coupled with the distribution of liquid oxygen phase before and after the occurrence of ignition, were carried out. Yang et al. [9] experimentally investigated cryogenic reactive coaxial sprays with oxygen and hydrogen or methane in order to determine if concepts from H_2/LOx injector design can be transferred to LOx/CH_4. The experimental study of the ignition and flame stabilization of a gaseous methane/oxygen jet for different configurations and injector conditions is described in [10].

In the present study, the numerical investigation of laminar CH_4/air as well as CH_4/O_2 flames in the counterflow configuration is performed in order to obtain a flamelet

* Corresponding author

library for turbulent combustion and to investigate principal differences between the LOx/CH_4 and the LOx/H_2 systems.

The combustion of laminar CH_4/air in the counterflow configuration is extensively studied in the literature. Several authors studied the behaviour of laminar CH_4/air in counterflow configurations at different conditions using different chemical reaction mechanisms. For instance, in [1] numerical results for laminar CH_4/air diffusion flames using a starting kinetic mechanism, a reduced 5-step mechanism and a 4-step mechanism, are presented. Other authors, [11, 12, 13 and 14] specifically studied the effect of enriched oxygen flames. For example, in [11] and [12], oxygen-enhanced methane counterflow flames were investigated through optical diagnostics and numerical simulations. The effect of strain rate and the influence of oxygen concentration in the oxidizer on the flame structure were studied for nitrogen-diluted methane (20% CH_4 and 80% N_2). The strain rate varies from 60 to 168s^{-1} while in the oxidizer stream, the nitrogen in air is replaced by oxygen ranging from 23% O_2 to 100% O_2. For the simulations, the GRI-Mech 3.0 chemical kinetic mechanism was used. In [14], soot formation in oxygen-rich counterflow for methane-oxygen diffusion flames was investigated. It was found that soot formation in methane flames is enhanced by oxygen enrichment. With increase of the oxygen in the oxidizer stream, the soot zone narrows and is shifted towards the stagnation plane. An extension of the GRI 2.11 mechanism including chemical reactions with species up to C_6, and thus consisting of 365 reactions among 62 chemical species was used. A soot map that separates non-soot from soot regions for laminar counterflow methane-oxygen-nitrogen diffusion flames at atmospheric pressure is given in [13]. Soot formation is studied at a constant strain rate of 20/s as a function of the methane content ranging from 25% to 100% in nitrogen in one stream and as a function of oxygen diluted in nitrogen from 35% to 100% in the oxidizer stream.

The purpose of the present paper is the numerical investigation of pure CH_4/O_2 and CH_4/air flames in the counterflow configuration at normal and elevated pressures and evaluation of their extinction conditions for use in turbulent flamelet computations. Moreover, the nitrogen/oxygen ratio is varied. Properties of methane at cryogenic inlet conditions are considered which are typical for liquid rocket propulsion systems. These properties are parameterized for use in future LOx/methane computations.

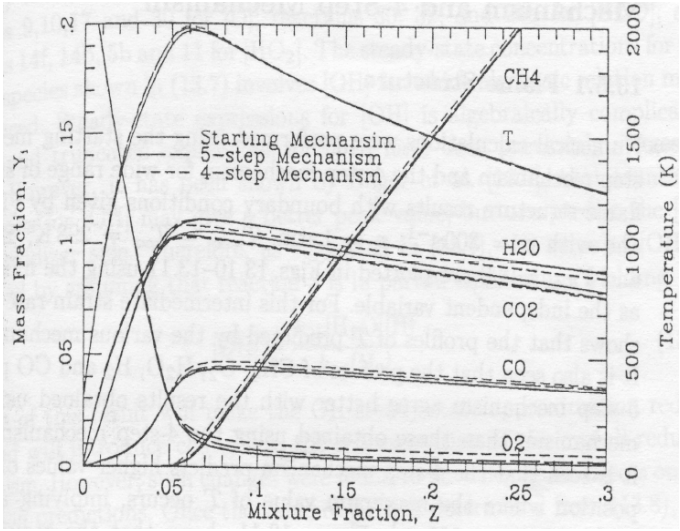

Fig. 1. Profiles of temperature and major species mass fractions for a CH_4/air flame at standard conditions [1] at a fuel-side strain rate of 300/s.

In the following, a short overview of the present mathematical model is given. Flame structures for CH4/O2 and CH4/air counterflow configuration are then presented and discussed.

MATHEMATICAL MODEL

An axisymmetric counterflow configuration is considered, where either gaseous or liquid fuel versus oxidizer, hot products, inert gas, may be fed from each side of the stagnation plane in any combination [15,16,18-20].

The mathematical model is based on Eulerian/Lagrangian formulation of non-dimensional equations [15,16], which are obtained using a similarity transformation transforming the two-dimensional equations into a one-dimensional system.

The gas-phase model includes a detailed chemical reaction mechanism [21] for CH_4/air and CH_4/O_2. It consists of 294 elementary reactions among 35 species. The gas phase transport coefficients are computed from NASA polynomials which cover the temperature range between 300 and 5000K.

The chemical reaction terms cause the system of conservation equations to be strongly non-linear and stiff. The system of equations is solved using a numerical scheme described in [15,16,18-20]. For the solution of the gas phase equations, an adaptive grid is used. The verification of the mathematical model and mechanism is achieved through comparison of the present results for CH_4/air and $CH_4/N_2/O_2$ flames with results from the literature [1,23].

RESULTS AND DISCUSSION

Both CH_4/air and CH_4/O_2 flames are studied as well as configurations with different mixture ratios of nitrogen and oxygen. The pure fuel comes from one side of the counterflow configuration whereas the oxygen/nitrogen mixtures are directed against the fuel stream. In order to validate the mathematical model, the results of the CH_4/air flame is compared with results from the literature [1, 23] as shown in Figures 1 through 4. In [1, 23], numerical results for CH_4/air diffusion flame were computed using a detailed starting kinetic mechanism, a reduced 5-step mechanism and a 4-step mechanism. The starting mechanism is a skeletal C_1

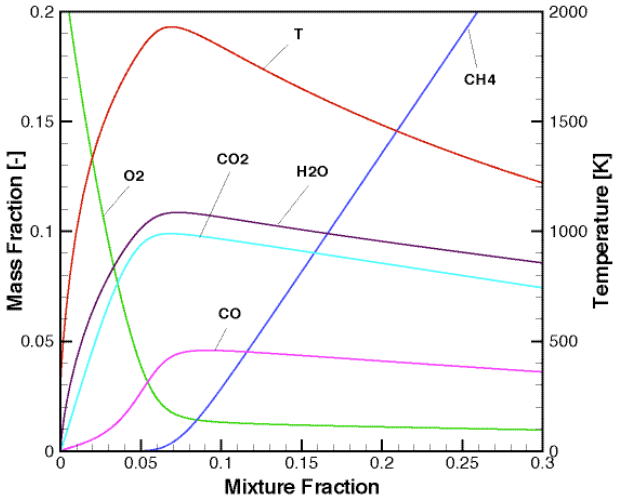

Fig. 2. Profiles of temperature and mass fractions of major species for a CH_4/air flame at standard conditions for a fuel-side strain rate of 300/s.

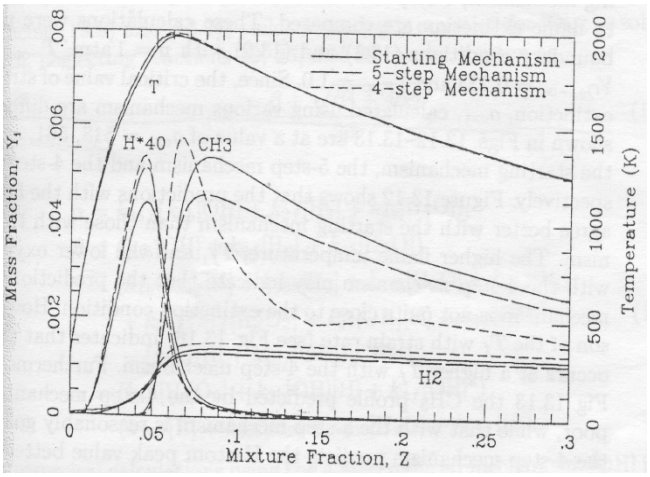

Fig. 3. Profiles of temperature and mass fractions of minor species mass fractions for CH_4/air [1] at strain rate 300/s.

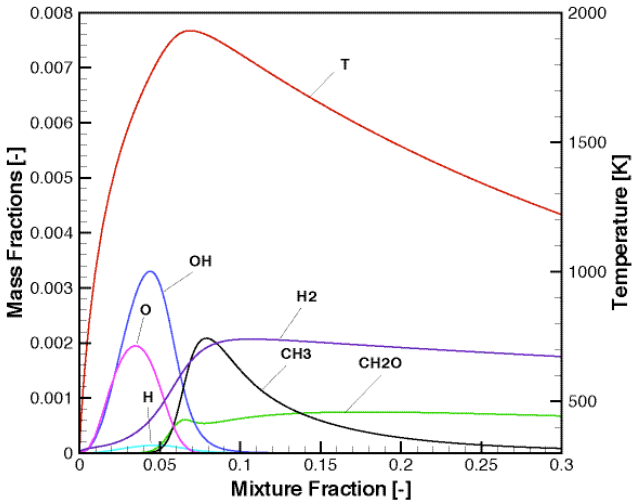

Fig. 4. Profiles of temperature and mass fractions of minor species mass fractions for CH_4/air at strain rate 300/s.

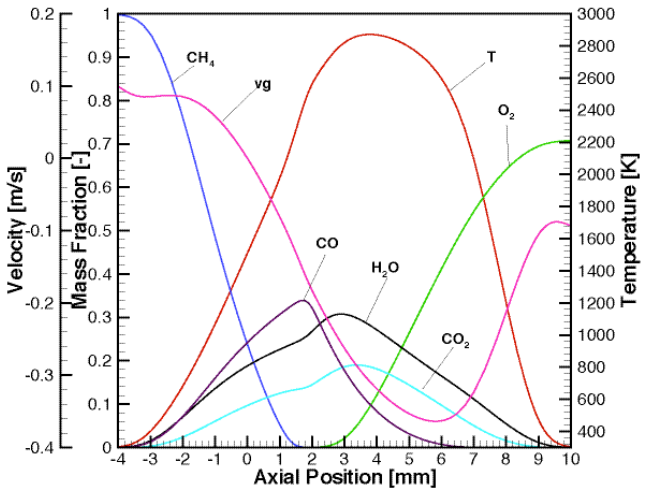

Fig. 5. Profiles of temperature and mass fractions of CH_4, O_2, H_2O, CO_2 and CO of a $CH_4/O_2/N_2$ flame at a fuel-side strain rate of 20/s.

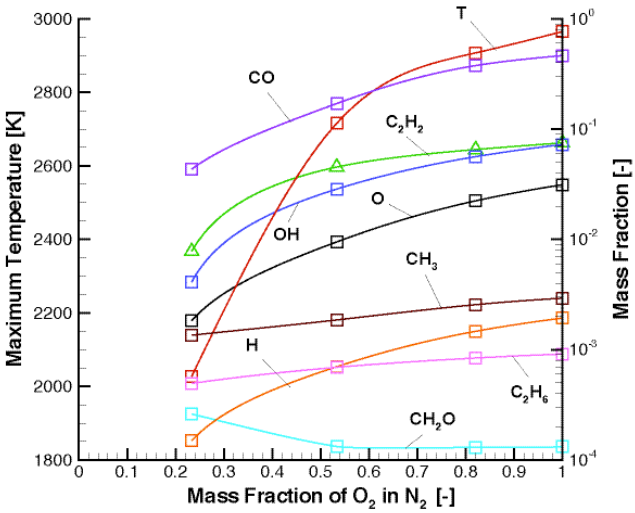

Fig. 6. Maximum flame temperature and mass fraction of various species with increase of oxygen content in the oxidizing stream at a strain rate of 100/s.

mechanism including 39 reactions among 17 species. Pure methane is directed versus an air stream. The strain rates at the fuel side range from 300/s to extinction. For the three different mechanisms in [1], the extinction strain rates are 518, 561, and 547s^{-1}, for the starting kinetic mechanism, 5-step and the 4-step mechanism, respectively, at standard conditions. The extinction temperature is approximately 2000K.

For verification of the code and the chemical reaction scheme, a comparison of a CH_4/air flame at standard conditions and a fuel-side strain rate of 300/s is computed. The comparison of the flame structure in the literature [1], c.f. Fig. 3, and the present simulations (see Fig. 4) shows an excellent agreement. The present simulations yield an extinction strain rate at the fuel side of 380/s and the extinction temperature is 1874 K. The major difference in the models is the employed chemical reaction scheme. The present mechanism includes C_2 reactions [21], which are neglected in Ref. [1]. In stoichiometric CH_4/air flames, the recombination path consumes about 20-30% of the CH_3 radical [21] and therefore the present mechanism includes these reaction rates. Figures 1-4 demonstrate a very good agreement between the present results and the data from the literature. The small discrepancies between the present simulations and the results presented in [1] may be due to the different mechanisms. The C_2 branch typically causes lower extinction temperatures due to the fact that more chemical species are involved leading to a reduced maximum gas temperature because of their energy content.

Next, laminar CH_4/O_2 flames are investigated. This is achieved through successive replacement of nitrogen through oxygen in the air stream opposing the methane flow. For a molar mixture of 68% O_2 and 32% nitrogen, there are results in the literature [14]. In [14], an extended GRI-Mech 2.11 chemical kinetic mechanism up to C_6 mechanism is used. The conditions in Ref. [14] are standard conditions, and the strain rate on the fuel side of the configuration is 20/s. Figure 5 shows the present results of the outer flame structure of this configuration using the Warnatz mechanims. They are in very good agreement with the results presented in [14]. For instance, in [14] the peak flame temperature is about 2800K, peak values of H_2O and H_2 mole fractions is about 0.38 and 0.2 while in the present simulation results the peak flame temperature is 2871K and the corresponding peak values of H_2O and H_2 are 0.38 and 0.21. Thus, the present code is suitable to represent all relevant results in the literature.

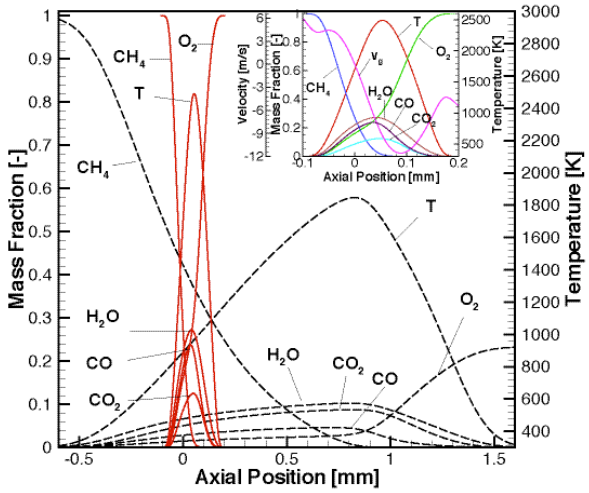

Fig. 7. Profiles of temperature and mass fractions of CH_4, O_2, H_2O, CO_2 and CO of a CH_4/air (black) and a CH_4/O_2 (red) flame at extinction. Zoomed figure for CH_4/O_2.

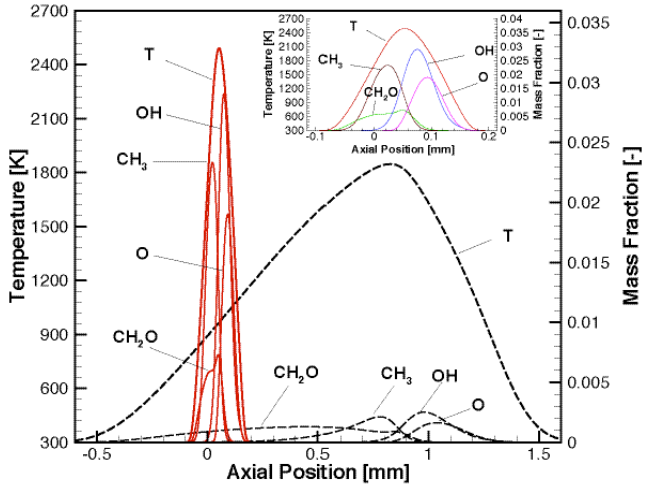

Fig. 8. Profiles of temperature and mass fractions of CH_3, CH_2O, OH and O for the CH_4/air (black) and the CH_4/O_2 (red) flame at extinction. Zoomed figure of CH_4/O_2.

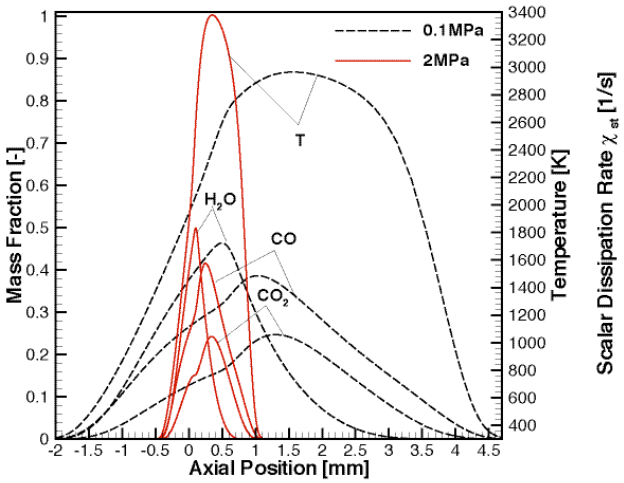

Fig. 9. Profiles of temperature and of mass fractions of H_2O, CO_2 and CO for the CH_4/O_2 flame at strain rate of 100/s and pressures of 0.1MPa and 2MPa.

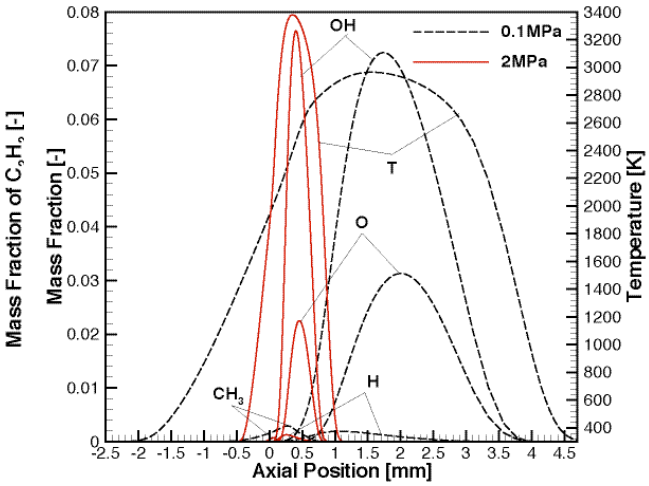

Fig. 10. Profiles of temperature and of mass fractions of CH_3, CH_2O, OH and O for the CH_4/O_2 flame at strain rate of 100/s and pressures of 0.1MPa and 2MPa.

Removal of nitrogen from the air stream was completed so that pure methane/oxygen flames are obtained. Figure 6 shows the maximum temperature and the mass fractions of species CH_3, CO, O, OH, C_2H_2, C_2H_6, H as well as CH_2O as a function of the oxygen mass fraction at a strain rate of 100/s. The oxygen mass fraction starts from 0.233 diluted in nitrogen (CH_4/air) to pure O_2. With an increase of oxygen content in the oxidizing gas stream, maximum flame temperature increases substantially from 1874 K to 2965 K. The maximum mass fraction of the major species plotted in Figure 6 increases non-linearly as nitrogen is removed from the system. At the same time, formaldehyde is decreased with nitrogen removal.

The pollutants and soot formation in laminar flames are of particular interest. The detailed chemical reaction mechanism used here is favourably enabled to predict formation of species such as CO, C_2H_2 as well as CH_2O. Maximum mass fraction of carbon monoxide and acetylene increase by a factor of about 10 as nitrogen is removed (CO increases from 0.043 to 0.46 and C_2H_2 from 0.0078 to 0.075, respectively). The maximum mass fraction of other species such as CH_2O is much smaller.

Figures 7 and 8 display a comparison of the outer flame structure of the CH_4/air (black) and the CH_4/O_2 (red) flames at the strain rates near extinction and standard conditions. The in-figures show an enlarged view of CH_4/O_2 flame for the same conditions. With replacement of nitrogen through oxygen, the flame thickness decreases dramatically by about a factor of seven. This is due to the fact that the damping of chemical reactions by nitrogen is removed with replacement of nitrogen through oxygen leading to enhanced chemical reactions. This enhancement is accompanied by a pronounced increase of flame temperature as can be seen in the figures. The increase of gas temperature leads to higher values of mass fraction for the major species in the chemical reaction system. In both systems it is observed that the flame resides on the oxidizer side of the flame which is typical for gas flames of this type. For the methane/oxygen flame, however, the flame is shifted towards the stagnation plane.

The extinction strain rate for CH_4/air flame is 380/s, and the corresponding value for the CH_4/O_2 flame is 46,750/s while the extinction temperature of the CH_4/air is 1874 K

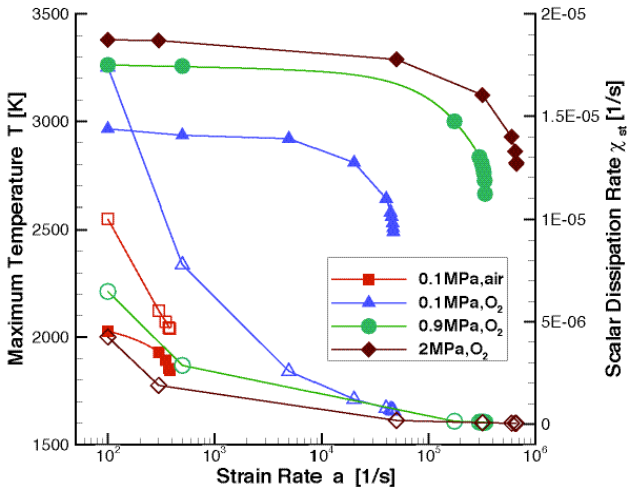

Fig. 11. Profiles of maximum temperature (filled symbols) and scalar dissipation rate (empty symbols) at strain rates up to extinction.

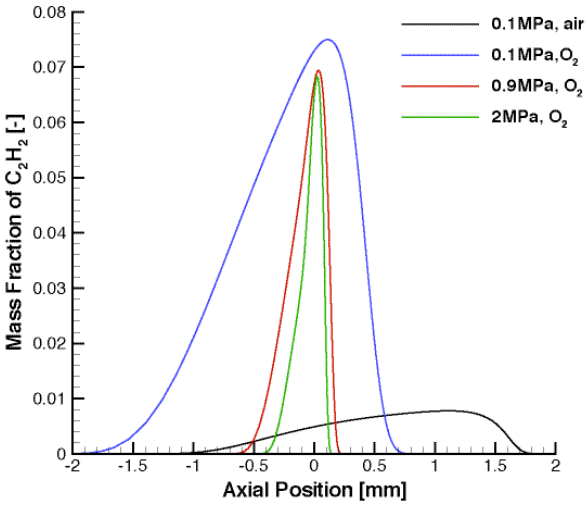

Fig. 12. Profiles of C_2H_2 mass fraction at different configurations and strain rates of 100/s.

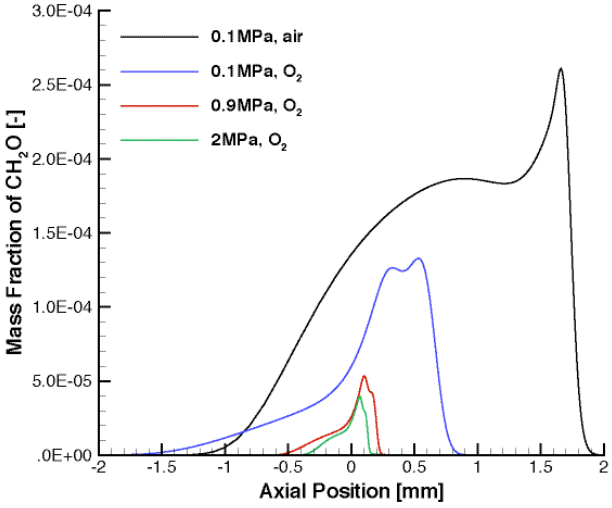

Fig. 13. Profiles of CH_2O mass fraction at different configurations and strain rates of $100s^{-1}$.

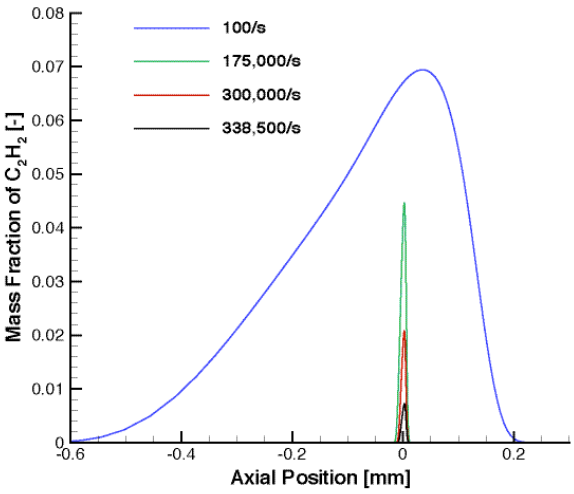

Fig. 14. Profiles of C_2H_2 mass fraction for CH_4/O_2 configuration at 0.9MPa and different strain rates.

versus 2,490 K for the CH_4/O_2 flame. Figure 7 also shows the profiles of the main reaction products H_2O, CO_2 and CO as well as the fuel and oxygen. It can be easily seen that in case the of the CH_4/O_2 flame, all the major species attain higher maximum values of all mass fractions compared to the CH_4/air flame as a consequence of the elevated flame temperature. In the CH_4/O_2 flame, the maximum mass fraction of H_2O is 0.27, that of CO_2 is 0.125, and the maximum mass fraction of CO is 0.237. The corresponding values for the CH_4/air flame are 0.1, 0.087, and 0.045, respectively.

Figure 8 displays the profiles of the species CH_3, CH_2O, O as well as OH. Oxygen containing species peak on the oxidizer side of the configuration whereas carbon containing species peak on the fuel side which is typical for this type of flames. In the case of CH_4/O_2 flame, the maxima of the mass fraction of all the minor species are higher than in case of CH_4/air flame. This is due to the fact that the extinction strain rate for the CH_4/O_2 flame is much higher than the extinction strain rate for CH_4/air flame. High strain rate reduces residence time and thus promotes formation of intermediate species as well as certain pollutants.

Figures 9 and 10 show the profiles of temperatures and major and minor species respectively, at a strain rate of 100/s and pressures of 0.1MPa and 2MPa. At elevated pressure, there is a pronounced increase of flame temperature and the flame thickness narrows. Peak values of radical concentrations show a pronounced increase as pressure increases.

Figure 11 shows results of the parametric study that was done to obtain a flamelet library. In flamelet computations, the scalar dissipation rate plays an important role since it is relevant to determine the regime of extinguished and burning flamelets. The scalar dissipation rate varies with space (and mixture fraction), and typically the flamelet computations include the value of scalar dissipation rate at stoichiometric conditions [24,25]. Therefore, the figure shows both maximum flame temperature, T, and scalar dissipation rate at stoichiometric conditions, χ_{st}. Besides the flames discussed

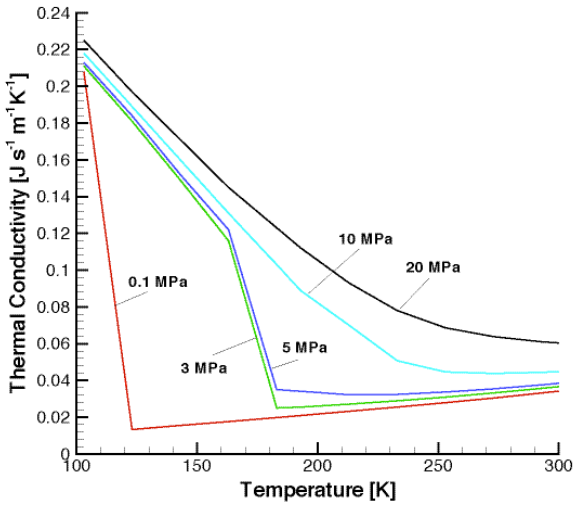

Fig. 15. Pressure and temperature dependence of thermal conductivity for methane in the temperature range 100≤T≤300K.

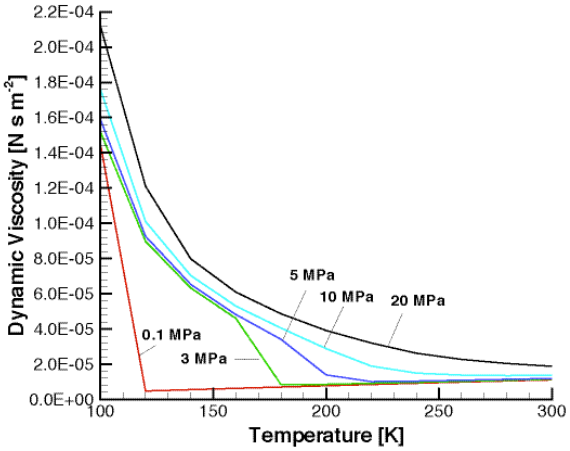

Fig. 16. Pressure and temperature dependence of dynamic viscosity for methane in the temperature range 100≤T≤300K.

so far, methane/oxygen flames at elevated pressures are investigated which are relevant for liquid rocket propulsion applications. In particular, the pressures 0.1, 0.9, and 2MPa are investigated. For all cases, extinction conditions are determined.

It is well known that increased pressure leads to increased flame stability and thus to increased extinction strain rates and temperatures. The extinction strain rate of methane/oxygen at 0.9MPa is found to be 338,500/s with extinction temperature of 2662K. For 2.0MPa the corresponding values are 667,500/s and 2801K. As extinction is approached, the temperature drop with increased strain is striking, and special attention needs to be taken to carefully evaluate extinction data. Scalar dissipation at stoichiometry decreases with increased strain rate over several orders of magnitude.

Figure 12 shows the profiles of mass fraction of C_2H_2 for CH_4/air at 0.1MPa and CH_4/O_2 at 0.1, 0.9 and 2MPa, at a fixed value of strain rate, 100/s. It can be seen that for CH_4/air at 0.1MPa, the mass fraction profile of C_2H_2 is broader and the peak is shifted to the oxidizer side in comparison with the CH_4/O_2 flame. Pressure increase causes a narrowing of flame thickness and thus a narrower profile of acetylene. For pressures up to 2MPa for the CH_4/O_2 flame, the maximum mass fraction of C_2H_2 decreases.

Figure 13 shows the profiles of mass fraction of CH_2O for the same conditions as in Fig. 12 at a fixed strain rate of 100/s. Here, both nitrogen removal and pressure increase cause lower profiles of formaldehyde.

Figure 14 shows the profiles of mass fraction of C_2H_2 for CH_4/O_2 at 0.9MPa, and for different strain rates. With increased strain rate, the mass fraction of C_2H_2 decreases and the narrower profiles are consequence of the decreased flame thickness with pressure increase.

The study provides flame structures of methane/oxygen flames in the counterflow configuration. Both extinction conditions and values of scalar dissipation rate at stoichiometric condition are presented for inclusion into future flamelet computations of turbulent reactive flows.

Figures 15 and 16 show properties of methane between 0.1 and 20MPa and cryogenic temperatures for use in future liquid oxygen/methane spray flames. Previous studies have shown that the liquid phase is dominant in characterizing both laminar and turbulent flames and they may not be neglected [26].

The physical properties for methane and oxygen are covered by the NASA data only above 300K. Therefore, the set of physical properties must be extended by data from the JSME tables [18] for the temperature range between 80 and 300K and for pressures up to 20MPa. In Figure 15 and Figure 16, a strong dependence of pressure and temperature of thermal conductivity and dynamic viscosity is seen.

CONCLUSION AND FUTURE RESEARCH

Both normal and high-pressure laminar flames structures of CH_4/air and CH_4/O_2 have been investigated. The present detailed chemical reaction mechanism for methane/air contains 35 species with 294 elementary reactions. In contrast to standard chemical kinetic mechanisms in the literature, the present study includes C_2 reactions, which enable the prediction of soot precursors such as acetylene. Validation of both the chemical kinetics as well as the numerics were performed through comparison of the CH_4/air flame characteristics such as extinction data and flame structure with results from literature [1,23]. The agreement is excellent. The extinction temperature in the present computations is somewhat smaller compared to the date from the literature due to the extended reaction scheme.

Simulations of CH_4/O_2 flames at elevated pressure have been performed for both low and increased strain rates, in particular, extinction conditions are determined. It is confirmed that increased pressure enhances combustion decreases flame thickness.

Future work concerns the simulation of LOx/CH_4 combustion in the counterflow configuration. Of particular interest are simulations for LOx/CH_4 laminar spray flame under different conditions such as different droplet sizes, equivalence ratios as well as strain rates. These are the most important parameters that play a crucial role in these systems.

ACKNOWLEDGMENTS

The authors gratefully acknowledge financial support from Deutsche Forschungsgemeinschaft (DFG) through research grants SFB 568 and SFB 359.

REFERENCES

[1] H. K. Chelliah, K. Seshadri, C. K. Law, In: Reduced Kinetic Mechanisms for Applications in Combustion Systems. (Ed.: N. Peters and B. Rogg), Springer, 15 Edition (1993).

[2] S. Zurbach, J.L. Thomas, P. Vuillermoz, L. Vingert, M. Habiballah. Recent advances on LOx/CH_4 combustion for liquid rocket engine injector. AIAA 38, (2002).

[3] S. Zurbach, J.L. Thomas, C. Verplancke, L. Vingert, M. Habiballah. Recent advances on LOx/CH_4 combustion for liquid rocket engine injector. AIAA 39, (2003).

[4] S. Candel, M. Juniper, G. Singla, P. Scouflaire, C. Rolon. Structure and dynamics of cryogenic flames at supercritical pressure. Combust. Sci. and Tech. 178, 161–192 (2006).

[5] G. Singla, P. Scouflaire, C. Rolon, Candel. Transcritical oxygen/transcritical or supercritical methane combustion. Proc. Combust. Inst. 30, 2921–2928 (2005).

[6] G. Singla, P. Scouflaire, C. Rolon, Candel. Flame stabilization in high pressure LOx/GH_2 and GCH4 combustion. Proc. Combust. Inst. 31, 2215–2222 (2007).

[7] F. Cuoco, B. Yang, M. Oschwald. Experimental investigation of LOx/H_2 and LOx/CH_4 coaxial sprays and flames. ISTS 24, (2004).

[8] F. Cuoco, B. Yang, C. Bruno, O.J. Haidn, M. Oschwald. Experimental investigation on LOx/CH_4 Ignition. AIAA 40, (2004).

[9] B. Yang, F. Cuoco, M. Oschwald. Atomitation and flames in LOx/H2 and LOx/CH_4 - spray combustion. J. of Propulsion and Power 23(4), 763–771 (2007).

[10] C Pauly. Laser ignition of gaseous CH_4/O_2 coaxial jet. Phd thesis, DLR, Lampoldshausen, (2006).

[11] Z. Cheng, A. Wehrmeyer, J. , R. W. Pitz, Experimental and Numerical Studies of Opposed Jet Oxygen-Enhanced Methane Diffusion Flames, Combust. Sci. and Tech. (178), 2145–2163 (2006).

[12] Z. Cheng, A. Wehrmeyer, J., R.W. Pitz. Oxygen-Enhanced High Temperature Laminare Flames. AIAA 42, Reno, Nevada (2004).

[13] S.V. Naik, N.M. Laurendeau, J.A. Cooke, M.D. Smooke. A Soot Map for Methane-Oxygen Counterflow Diffusion Flames. Combust. Sci. and Tech. 175, 1165–1167 (2003).

[14] A. Beltrame, P. Porshnev, W. Merchan-Merchan, A. Saveliev, A. Fridman, L.A. Kennedy, O. Petrova, S. Zhdanok, F. Amouri, O. Charon. Soot and NO Formation in Methane-Oxygen Enriched Diffusion Flames. Combust. And Flame 124, 295–310 (2001).

[15] G. Continillo, W. A. Sirignano, Counterflow Spray Combustion Modeling, Comb. Flame 81, 325-340 (1990).

[16] E. Gutheil, W. A. Sirignano, Counterflow Spray Combustion Modeling Including Detalied Transport and Detailed Chemistry. Comb. Flame 113, 92-105 (1998).

[17] G. Abramzon, W. A. Sirignano, Droplet Vaporization Model for Spray Combustion Calculations. Int. J. Heat Mass Transfer 9, 1605-1618 (1989).

[18] D. Schlotz, E. Gutheil, Modeling of Laminar Mono- and Bidisperse Liquid Oxygen/Hydrogen Spray Flames in the Counterflow Configuration, Combust. Sci. Tech. 158, 195–210 (2000).

[19] E. Gutheil, Combustion Theory and Modeling 5, 1-15 (2001).

[20] E. Gutheil, Progress in Computational Fluid Dynamics, Vol. 5 No. 7, 414-419 (2005).

[21] J. Warnatz, U. Maas, R. W. Dibble, Combustion, Physical and Chemical fundamentals, Modeling and Simulation, Experiments, Pollutant Formation, Springer-Verlag, Berlin Heidelberg, New York, 2nd Edition, 1999.

[22] J. S. M. E., Data Book, Thermophysical Properties of Fluids, 1983.

[23] M. Bollig, A Linan, Sanchez, A.L., F.A. Williams. A simplified approach to the numerical description of CH4/Air diffusion flames. Proc. Combust. Inst. 27, 595–603 (1998).

[24] N. Peters, Laminar Flamelet Model of Turbulent Combustion in: Numerical Simulation of Combustion Phenomena, K. Bray, Ed., Lecture Notes in Physics, Springer, 2006.

[25] C. Hollmann, E. Gutheil, Modeling of Turbulent Spray Diffusion Flames Including Detailed Chemistry, Proc. Combust. Inst. 26, Vol. 1, 1731-1738 (1996).

[26] C. Hollmann, E. Gutheil, Flamelet-Modeling of Turbulent Spray Diffusion Flames Based on a Laminar Spray Flame Library, Combustion Science and Technology: 135, 1-6, 175 (1998).